# The effect of petrographically determined parameters on reductant reactivity in the production of high-carbon ferromanganese

by S. Soqinase[1,2], J.D Steenkamp[1,2], P. den Hoed[2], and N. Wagner[3]

**Affiliation:**
[1]Mintek, Randburg, South Africa
[2]Department of Chemical and Metallurgical Engineering, University of the Witwatersrand, Johannesburg, South Africa.
[3]DSI-NRF CIMERA, Department of Geology, University of Johannesburg, Johannesburg, South Africa.

**Correspondence to:**
S. Soqinase

**Email:**
sandas@mintek.co.za

**Dates:**
Received: 19 Sep. 2022
Accepted: 31 Jan. 2023
Published: February 2023

**How to cite:**
Soqinase, S., Steenkamp, J.D., den Hoed, P., and Wagner, N. 2023 The effect of petrographically determined parameters on reductant reactivity in the production of high-carbon ferromanganese. Journal of the Southern African Institute of Mining and Metallurgy, vol. 123, no. 2, pp. 71–80

**DOI ID:**
http://dx.doi.org/10.17159/2411-9717/2321/2023

## Synopsis

**In pyrometallurgical processes, metal oxides are reduced from molten slag through carbothermic reduction. It is of interest to evaluate the reactivity of the carbonaceous materials towards substances such as slag. Characterization techniques such as coal petrography can provide insight into the influence of feed coal properties and how they potentially dictate reductant performance. This study aimed to compare the petrographically determined organic composition of coal to reductant reactivity. Two South African medium-rank C bituminous coals and one anthracite sample were investigated together with high-carbon ferromanganese industrial slag. The reductant reactivity tests were conducted at 1500°C in a muffle furnace to assess the potential of carbonaceous reductant in reacting with the main slag components. SEM-EDS was applied to understand the extent of MnO (and to a lesser extent, $SiO_2$) reduction from the slag. Coal 2, consisting of a greater proportion of vitrinite (59.5 vol% on a mineral matter-free basis and 54.7 vol% including mineral matter) was the most reactive reductant. The anthracite sample, with the highest inert maceral proportions (71.8 vol% including mineral matter and 76.8 vol% on a mineral matter-free basis), was the least reactive reductant.**

## Keywords

**reductant reactivity, MnO reduction, coal petrography, high-carbon ferromanganese slag.**

## Introduction

High-carbon ferromanganese (HCFeMn) is a manganese alloy commonly produced in submerged arc furnaces (SAFs) in which metal oxides are reduced by carbon, from coke or coal char, to form a slag phase (Ostrovski and Swinbourne, 2013). Excavation of an industrial HCFeMn SAF revealed different reaction zones within the furnace interior (Olsen and Tangstad, 2004; Ringdalen, Tangstad, and Brynjulfsen, 2015). The two main reaction zones are the prereduction zone, where the charge is solid, and the coke bed zone, where ore, slag, and fluxes are molten (Olsen and Tangstad, 2004). There are two possible mechanisms of MnO*x* reduction suggested, which are indirect reduction through the gas phase and direct reduction at the interface between carbon and slag (Rankin and Deventer, 1980; Rankin and Wynnyckyj, 1997). The reduction of the higher manganese oxide compounds to MnO occurs through the release of upflowing CO gas in the pre-reduction zone (Suharno *et al.*, 2018). The main reaction in the coke-bed zone is the reduction of MnO from liquid slag, by either solid carbon or solute carbon, to form metallic manganese (Kim, 2018; Lindstad, Tangstad, and Olsen, 2007) as seen in Equation [1].

$$(MnO)_{(l)} + C = Mn_{(l)} + CO_{(g)} \quad [1]$$

The reaction ultimately controls the distribution of manganese between slag and alloy (Ringdalen and Tangstad, 2009). Various parameters have a bearing on the rate of carbothermic reduction of MnO from liquid slags. The parameters studied, are influenced by the reaction kinetics and thermodynamics, including temperature (Olso, Tangstad, and Olsen, 1998), slag composition, the basicity of the slag (Kolbeinsen *et al.*, 2006), and activity of MnO in slag. Several studies have been conducted to understand the mechanisms of MnO reduction by carbon from high-carbon ferromanganese slags (Rankin and van Deventer, 1980; Coetsee, 2018; Safarian *et al.*, 2008, 2009; Sun *et al.*, 2010 ; Safarian and Tangstad, 2010).

The significance of carbonaceous reductant is its role in the reduction of oxide compounds through the gasification of reductant and direct reduction of slag with solid carbon. Direct reduction relates to the reaction between the carbonaceous reductant and molten slag (Sahajwalla, Dubikova, and Khanna, 2004; Pistorius, 2002). Generally, reactivity refers to the rate at which a substance can undergo a reaction (Safarian and Tangstad, 2010). Since carbonaceous materials are frequently used in pyrometallurgical processes, it is important to define the reactivity of carbon with specific substances. Reductant reactivity towards slag is defined as the potential of the carbonaceous reductant to react with the main slag components, specifically MnO.

### *Significance of petrographic analysis in coal utilization*

Relating reactivity to petrographically determined constituents is essential to understand the influence of feed coals and how they potentially perform in technological applications. The organic constituents of coal, known as macerals, are formed through biochemical and physicochemical changes in plant matter (Diessel, 1992) and, in turn, form the fundamental basis for petrographic assessment. Each maceral is distinguished by a unique set of physical, chemical, and technological properties for a given rank (Chen and Ma, 2002) which ultimately contribute to the behaviour of the coal. Generally, macerals are divided into reactive and unreactive groups based on changes in structure and chemical composition when heated. Reactive macerals soften, swell, and release volatile matter upon heating, while the inert forms of inertinite macerals at any rank will not combust easily and require more heat (Falcon and Ham, 1988).

The changes in the chemical reactivity and structure of the coal's organic constituents when heated needs to be considered when choosing a carbonaceous reductant since the resulting reductant will reflect the characteristics of the original coal. Extensive research data is available on the structural transformation of macerals and their change in chemical reactivity during processes such as pyrolysis and carbonization. For instance, the metallurgical industry depends on the petrographic assessment of coal for processes such as carbonization to produce quality coke. The thermal behaviour of particles extracted from pyrolysis, combustion, or gasification processes can be assessed petrographically (Bunt, Wagner, and Waanders, 2009; Malumbazo, Wagner, and Bunt, 2012; Alonso *et al.*, 2001). Reactive macerals are known to devolatilize easily with increasing temperature and rank (Falcon and Ham, 1988), consequently swelling and becoming porous. Contrastingly, the principal unreactive maceral such as inertinite undergo little to no change in structure upon heating. This is true for reductant types irrespective of coal rank. Inertinites are generally poor in volatiles, and will not swell and become porous at any temperature, due to their dense structure.

It is, therefore, essential to establish the key characteristics of the carbonaceous reductants that influence reductant reactivity towards slag, for selection in the production of HCFeMn. Such a study should include intrinsic coal properties, such as the organic composition, and how they could potentially perform at high temperatures for use as carbonaceous reductants. Understanding the underlying reasons for the variations in feed carbons and how suitable each will be as a reductant for each process is important.

## Experimental procedure

Three reductant samples were sourced from a South African producer of manganese ferroalloys. The samples are described as coal 1, coal 2, and anthracite. The industrial HCFeMn slag sample used was sourced from one of South Africa's HCFeMn producers.

### *Chemical analysis*

The bulk chemical composition of the HCFeMn slag sample (Table I) was determined by inductively coupled plasma optical emission spectrometry (ICP-OES).

The bulk chemical compositions of the prepared representative coal samples were determined by proximate analysis using standard methods to measure moisture, ash, fixed carbon (by difference), and volatile matter (Table II).

### *Specific phase chemical analysis*

SEM-EDS was used for the identification of specific phases in the as-received slag phase and heat-treated slag sample microstructures at different reaction times to assess the extent of reduction. The SEM instrument used was a ZEISS Sigma 300VP with a field emission gun and ZEISS 'Smart SEM software. The EDS detector used was an Oxford Instruments X-act PentaFET Precision with Oxford INCA software.

### *Petrographic analysis*

Representative coal samples (coal 1, coal 2, and anthracite) were crushed and mixed in epoxy resin and prepared as polished sections in accordance with ISO 7404-2. The petrographic analysis was carried out under oil immersion using a Zeiss Axio Imager M2m petrographic microscope fitted with a Fossil Hilgers system, at a magnification of 500×. Maceral group analysis and rank determination were conducted following SABS ISO 7404 parts 3 and 5 respectively.

### *Equipment*

The carbonaceous reductant reactivity tests were conducted in an Ultrafurn gas-tight muffle furnace (Figure 1), with workable chamber dimensions (H × W × D) of 175 mm × 195 mm × 175 mm, equipped with molybdenum disilicide (MoSi2) heating elements. A CAHO P961 programmable controller was used to set the heating

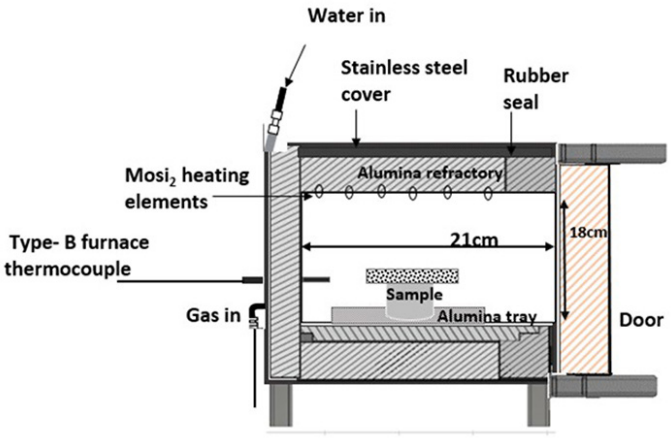


**Figure 1—Schematic diagram of gas-tight furnace set-up used for the carbonaceous reductant reactivity tests**

rate of 10°C/min to the target reaction time and set temperature. The reactivity test matrixes, one for each reductant, with the HCFeMn slag heated to 1500°C for periods of 72 to 360 minutes at 72-minute intervals are presented in Table III.

Crucibles were prepared from large lumps of each carbonaceous reductant type (dimensions 25-27 mm inner diameter, 7-10 mm thickness, and height 50 mm) as seen in Figure 2. Once prepared, the reductant crucibles were filled with slag. The combined mass of the crucible and slag was recorded. The mass of the slag before the reaction was determined by difference. The charged crucibles were placed into size A5 alumina crucibles, which served as containment vessels in case of leakages, and aided in positioning the crucibles in the furnace chamber. To scavenge any oxygen that could potentially enter the chamber, a refractory board, with reactive carbon placed on top, was used as a lid to the alumina crucible.

The furnace was heated gradually at a rate of 10°C/min to 1500°C under an inert atmosphere. Once the reaction time lapsed, heating was stopped. The sample was kept inside the chamber and allowed to cool overnight to room temperature while the argon gas flowed continuously. Once cooled, the reacted reductant crucible plus slag was removed from the alumina crucible and the combined mass of the crucible and slag was determined by weighing. The mass of slag and reductant after reaction allowed for the determination of mass loss percentage (Equation [2]) as a function of reaction time.

$$Mass\ loss\ \% = \frac{\Delta m}{m_i} x100 \qquad [2]$$

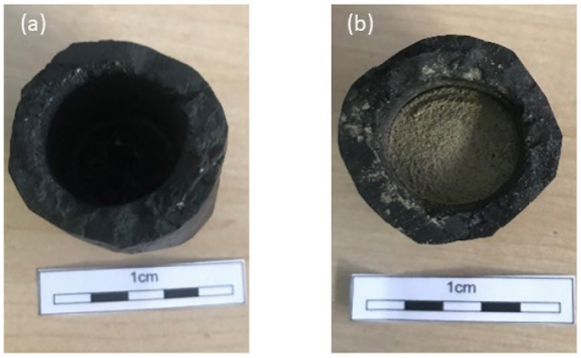


**Figure 2—(a) Reductant crucible prepared from the large coal lumps (b) filled with HCFeMn slag**

where
$\Delta m$ = (Initial mass of reductant crucible + slag) – (final mass of reductant crucible + slag) (g)
$m_i$ = initial mass of reductant crucible + slag (g)

## Results and discussion

### *Material characterization*

### *Chemical analysis*

The representative HCFeMn slag sample was analysed by ICP-OES. The slag bulk chemical analysis indicated an average MnO content of 23.4% (Table I).

The proximate analysis for the parent coal samples is provided in Table II. The results indicate that the volatile matter was the highest in coal 2 at 29.3, followed by coal 1 at 27.7%. The anthracite sample had the least volatile matter at 5.4% and the highest fixed carbon (78.1%). The moisture and ash contents were similar in all three parent coals. The moisture contents ranged between 3.2% and 3.9% and the ash yield between 16.3% and 17.4%.

### *Specific phase chemical analysis*

The specific phase chemical analysis results quantified by SEM-EDS for the as-received HCFeMn slag are presented in Figure 3. The

*Table I*

**Bulk chemical composition of the HCFeMn slag by ICP-OES (%)**

| Sample ID | MnO | FeO | CaO | MgO | $SiO_2$ | $Al_2O_3$ | $K_2O$ | $TiO_2$ | BaO |
|---|---|---|---|---|---|---|---|---|---|
| Average | 23.4 | 0.8 | 29.4 | 7.1 | 34.5 | 3.9 | 0.2 | 0.2 | 0.6 |
| Std dev. | 0.36 | 0.05 | 0.34 | 0.16 | 0.25 | 0.04 | 0.01 | 0.00 | 0.01 |

*Table II*

**Proximate data for the coals tested**

| | Proximate analysis (% dry basis) | | | |
|---|---|---|---|---|
| Sample | Moisture | Volatile matter | Ash | Fixed carbon |
| Coal 1 | 3.2 | 27.7 | 16.3 | 55.0 |
| Coal 2 | 3.9 | 29.3 | 17.4 | 52.1 |
| Anthracite | 3.9 | 5.4 | 16.3 | 78.1 |

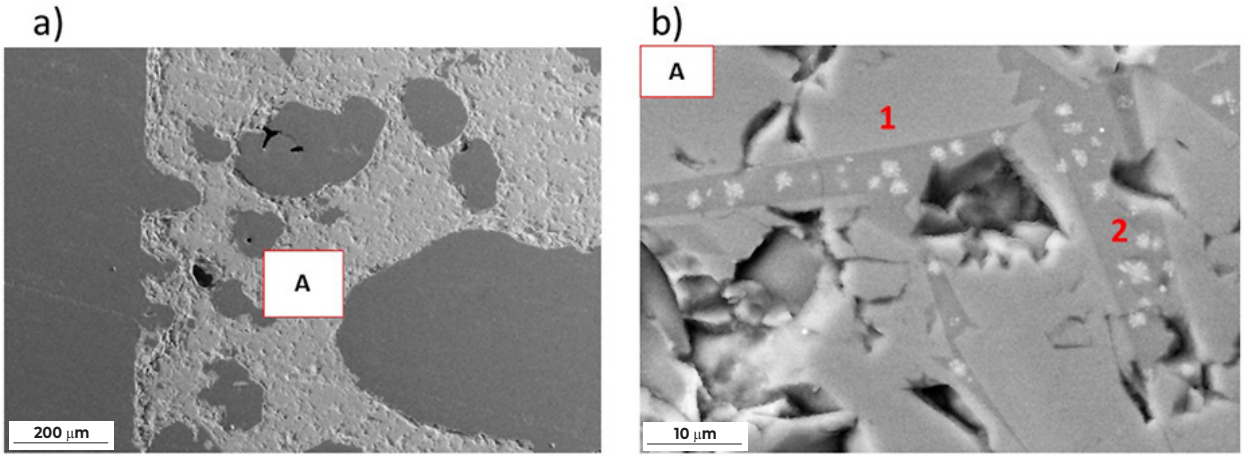


**Figure 3—SEM micrographs of the as-received HCFeMn slag , acquired at 20.0 kV. (a) Secondary electron image, Scale bar indicates 200 µm. (b) Backscattered electron image of area A of primary phase (1) and secondary phase (2). Scale bar indicates 10 µm**

analysis revealed two phases –a primary phase and a secondary phase. The primary phase had a higher $SiO_2$ content while the secondary phase had a higher MnO content. On average the two phases consisted of 27.3% MnO and 32.8% $SiO_2$.

The Fe-Mn-C alloy in the as-received slag (Figure 4) consisted predominantly of Fe at greater than 80 wt.%. Fe in the as-received slag is indicative of the presence of a metallic phase in the slag. The presence of metallic Fe in the system has been shown to accelerate the carbon/slag interactions (Teasdale and Hayes, 2005).

### *Petrographic analysis*

The reflectance measurement results of the parent samples (Table IV) classified coal 1 and coal 2 as medium-rank C bituminous coals. The anthracite sample is classified as high-rank coal with a vitrinite reflectance measurement of 2.9 RoVmr%. The classification follows the international classification of in-seam coals (United Nations Economic Commission for Europe, 1998).

The boundaries that separate the different categories of coal rank are justified by important changes in coal properties or behaviour (Pinheiro, 2006). Volatile matter and fixed carbon are found to have opposing effects (Figure 5). Generally, as rank increases, volatile matter content decreases, leading to a reciprocal carbon content enrichment due to the geochemical changes the coal undergoes with the progression of rank.

The maceral data in Table IV indicates that coal 1 and coal 2 are vitrinite-rich: 44.3 vol.% on a mineral matter free basis and 40.5 vol.% including mineral matter in coal 1, and 59.3 vol.% 54.7 vol.% respectively in coal 2. The anthracite sample has the least vitrinite proportion of 21.3 vol.% including mineral matter and 22.8 vol. % on a mineral matter-free basis and is inertinite-rich. Liptinite content was very low at 0.4 to 4.7 vol.% on both a mineral matter-free basis and including mineral matter. The vitrinite in coal 1 and coal 2 is mainly dominated by bands of collotelinite and collodetrinite as seen in Figure 6 and Table IV. The principal inertinite maceral is inert semifusinite with anthracite comprising the highest proportion.

The total reactive macerals are made up of vitrinite, liptinite, reactive semifusinite, and reactive inertodetrinite. Coal 1 and coal 2 displayed a higher total reactive maceral content compared to anthracite. Coal 1 consisted of 55.2 vol.% total reactive macerals on a mineral matter-free basis and 50.5 vol.% including mineral matter. Coal 2 consisted of 64.5 vol.% on a mineral matter-free basis and 59.5 vol.% including mineral matter. The total inert macerals were the highest in nthracite at 76.8 vol.% on a mineral matter-free basis and 71.8 vol.% including mineral matter.

The series of micrographs in Figure 6 identifies the dominant macerals.

### *Reactivity tests*

The results in Figure 7 show that after 72 minutes of reaction time, coal 2 exhibited the highest initial mass loss of 38.6%. Coal 1 lost 32.9%, and anthracite had the least mass loss at 12.1%. The initial

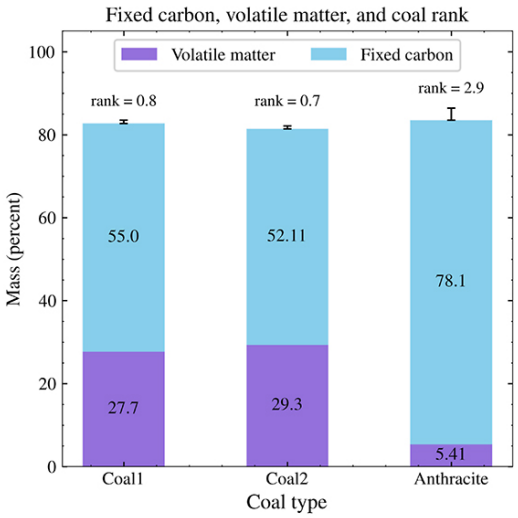


**Figure 5—Coal rank relationship with volatile matter and fixed carbon for the coals studied**

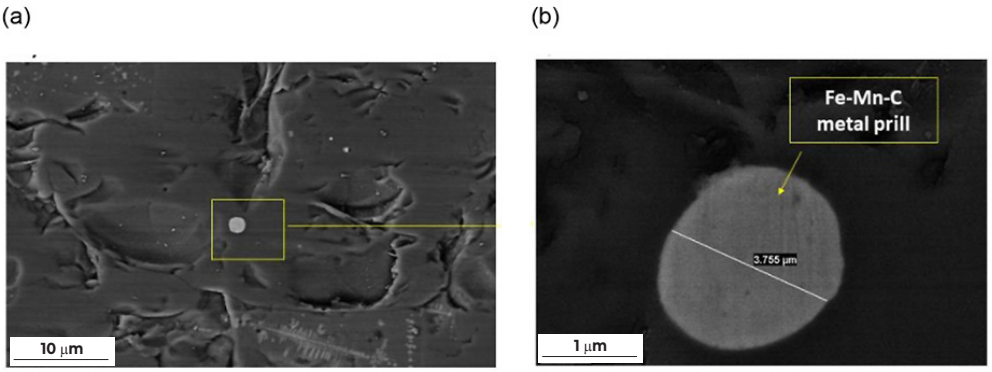


**Figure 4—Backscattered electron images acquired at 15.0 kV. (a) Metal prill entrained in the feed , consisting of Fe metal. Scale bars indicate 10 µm (a) and 1 µm (b)**

*Table III*

**Reactivity test matrixes**

| Raw materials | Temperature (°C) | Reaction times (min) |
|---|---|---|
| HCFeMn slag and anthracite | 1500 | 72, 144, 216, 288, 360 |
| HCFeMn slag and coal 1 | 1500 | 72, 144, 216, 288, 360 |
| HCFeMn slag and coal 2 | 1500 | 72, 144, 216, 288, 360 |

*Table IV*

**Maceral group composition (vol.%) and reflectance results (mmf: mineral matterfree basis, Inc. mm: including mineral matter)**

| Maceral group (vol. %) | Coal 1 | | Coal 2 | | Anthracite | |
|---|---|---|---|---|---|---|
| | *mmf* | *Inc. mm* | *mmf* | *Inc. mm* | *mmf* | *Inc. mm* |
| **Vitrinite** | 44.3 | 40.5 | 59.3 | 54.7 | 22.8 | 21.3 |
| Collotelinite | 24.1 | 22.0 | 33.6 | 31.0 | 13.9 | 13.0 |
| Collodetrinite | 19.2 | 17.5 | 23.9 | 22.0 | 8.4 | 7.9 |
| Corpogelinite | 0.4 | 0.4 | 1.4 | 1.3 | 0.2 | 0.2 |
| Telinite | 0.4 | 0.4 | 0.2 | 0.2 | 0.0 | 0.0 |
| Pseudovitrinite | 0.2 | 0.2 | 0.2 | 0.2 | 0.2 | 0.2 |
| **Liptinite** | 4.7 | 4.3 | 3.1 | 2.9 | 0.4 | 0.4 |
| Sporinite | 4.3 | 3.9 | 2.7 | 2.5 | 0.4 | 0.4 |
| Cutinite | 0.4 | 0.4 | 0.4 | 0.4 | 0.0 | 0.0 |
| **Inertinite** | 51.0 | 46.6 | 37.6 | 34.6 | 76.8 | 71.8 |
| Fusinite | 14.5 | 13.3 | 8.3 | 7.6 | 3.4 | 3.2 |
| Reactive semifusinite | 6.0 | 5.5 | 1.9 | 1.7 | 1.5 | 1.4 |
| Inert semifusinite | 21.7 | 19.9 | 20.3 | 18.7 | 58.6 | 54.8 |
| Inert inertodetrinite | 7.9 | 7.2 | 6.6 | 6.1 | 9.1 | 8.5 |
| Reactive inertodetrinite | 0.2 | 0.2 | 0.2 | 0.2 | 0.2 | 0.2 |
| Secretinite | 0.6 | 0.6 | 0.2 | 0.2 | 4.0 | 3.7 |
| **Mineral matter** | | 8.6 | | 7.8 | | 6.5 |
| Rank (mean random reflectance %) | 0.8 | | 0.7 | | 2.9 | |
| Rank category | **Med. rank C bituminous** | | **Med. rank C bituminous** | | **Anthracite** | |
| Total* reactive macerals | 55.2 | 50.5 | 64.5 | 59.5 | 24.9 | 23.3 |
| Total inert macerals | 51.0 | 46.6 | 37.6 | 34.6 | 76.8 | 71.8 |

*Total reactive macerals = vitrinite + liptinite + reactive semifusinite and reactive inertodetrinite

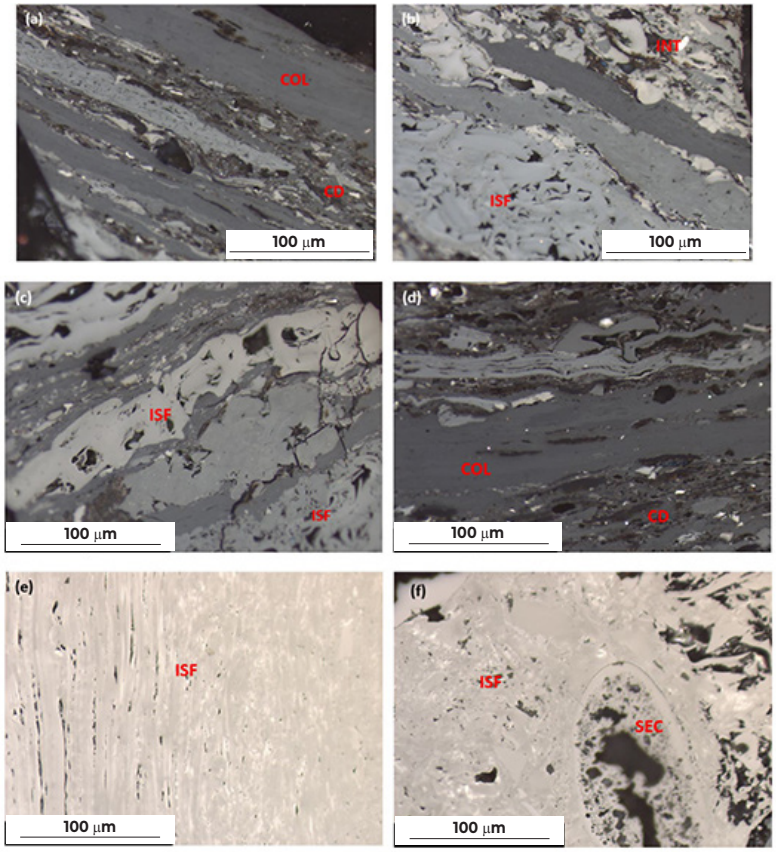


**Figure 6—Micrographs of coal 1 macerals (magnification 500× under oil immersion, reflected light). (a) Banded, vitrinite bands (collotelinite) and collodetrinite with a vitrinic groundmass and inertinite fragments, (b) smoother band of collotelinite surrounded by inert semifusinite and inertodetrinite, (c) coal 2 images of bands of semifusinite and vitrinite, (d) collotelinite and collodetrinite with a vitrinitic matrix and semifusinite, (e) anthracite images of banded semifusinite at different . (f) secretinite embedded within semifusinite showing internal. Scale bar indicates 100 µm**

| Time (min | Coal 1 | Coal 2 | Anthracite |
|---|---|---|---|
| 0 | 0 | 0 | 0 |
| 72 | 12.1 | 32.9 | 38.6 |
| 144 | 16.4 | 37.0 | 32.8 |
| 216 | 27.2 | 39.7 | 38.0 |
| 288 | 21.8 | 34.9 | 41.2 |
| 360 | 19.4 | 39.0 | 39.6 |

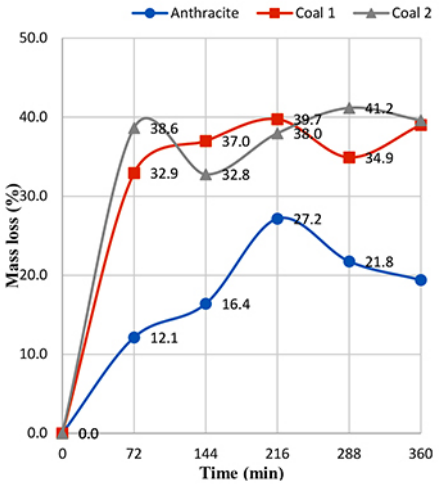


**Figure 7—Mass loss data and curves Please see the comment opposite**

rapid mass loss in coals 1 and 2 can be attributed to the release of volatile matter, which is expected to be driven off at temperatures above 400°C (Speight, 2015). The least initial mass loss observed in anthracite is related to the least volatile matter content (Table III).

Thereafter, coal 1 recorded a higher mass loss of 37.0% at 144 minutes and 39.7% at 216 minutes reaction time, compared to 32.8% and 39.7% for coal 2. At 288 and 360 minutes reaction time, the respective mass losses were 41.2% and 39.6% (coal 2) and 34.9% and 39.0% (coal 1). Anthracite underwent the least mass loss at all the reaction times. An almost linear mass loss pattern was observed for anthracite until 216 minutes. Moreover, a linear mass loss was noted in coal 1 at 72-216 minutes reaction time (32.9–39.7%). At higher temperatures, the mass loss was attributed to reduction of MnO in the slag to Mn in the alloy, which is expected to occur at temperatures between 1400 and 1500°C (Ringdalen, Tangstad, and Brynjulfsen, 2015).

The differences in reactivities of the reductants at the different reaction times can be attributed to several reasons. In Figure 8, the mass loss profile highlights the influence of the slag and reductant crucible sizes on the mass loss. In coal 2, less mass loss was observed at 144 and 216 minutes compared to the initial 72 minutes reaction time. This is attributed to the reductant crucible mass as seen in Figure 8, where less mass was consumed compared to the preceding 72 minutes reaction time. At 360 minutes reaction time, lower mass loss was also observed compared to 288 minutes reaction time. This is also due to the lower reductant crucible mass.

In contrast, anthracite underwent less mass loss at 288 and 360 minutes compared to the preceding 216 minutes due to the lower slag mass used. Besides the variable reductant crucible and slag masses, other factors such as the method used could have contributed to the sometimes nonlinear mass loss trend observed as a function of time. In addition, the tests were conducted in batch mode and not continuous as in the case of thermogravimetry-type tests. However, despite the stated reasons, the results demonstrate that overall coal 2 underwent the highest mass loss, followed by coal 1 and anthracite with the least mass loss. This ultimately translates to coal 2 being the most reactive carbonaceous reductant, followed by coal 1, and anthracite being the least reactive.

## *Characterization of post-mortem samples*

### *Macroscopic observations*

Cross-section images with corresponding observations at the different reaction times are presented in Figure 9.

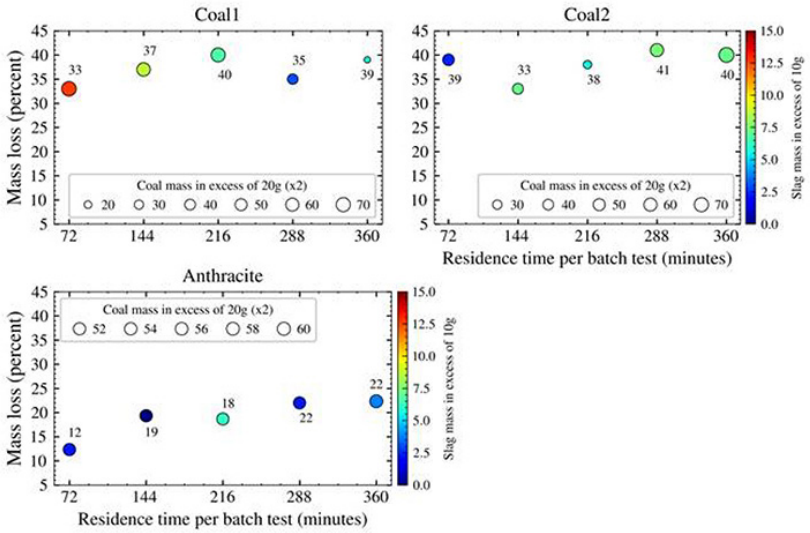


**Figure 8—Mass loss as a function of residence time with coal and slag mass differences**

- Coal 1 and coal 2 had similar appearances (with minor variations) compared to the anthracite, which reacted differently.
- Overall, and applicable to all the reaction times, coal 1 exhibited more heat-induced cracks and was found to be more porous and brittle to the touch. As a result, most of the slag penetrated through the cracks and settled at the base of the reductant 'crucible' or deposited within the cracks. Consequently, it was almost impossible to separate it from the alumina crucible that was serving as a containment vessel.
- The slag is characterized by a green colour, which indicates the presence of MnO. In the case of coals 1 and 2 the green slag disappeared after 72 minutes reaction time, which is an indication that there was little or no MnO present. The MnO could either have reacted with the carbon and reported as Mn in the alloy or been lost as part of the volatiles.
- In anthracite the change in slag colour from green to grey took place over longer reaction times compared to the coals.


**Figure 9—Cross-section images of the heat-treated samples at different reaction times**

This is in agreement with the reductant reactivity tests, where anthracite was seemingly the least reactive of the reductants.

- The volume and shape changes in anthracite after heat treatment were also less marked compared to the coals.

### *Specific phase chemical analysis*

- The results in Figure 10 show that at 72 minutes reaction time, the alloy in coal 1 was mostly present in the slag matrix, with two phases of Si-Mn-C. The slag microstructure differed from that of the as-received sample in that it consisted of a needle-like crystalline phase in a random network of veins.
- In coal 2 at 72 minutes reaction time the interface between the coal and slag was clearly defined with alloy forming in between. The coal was porous with metal entrainment between the pores. The alloy was identified as a single-phase alloy.
- The slag-anthracite interface is clearly defined with alloy preferentially located between the slag and carbon. The alloy consisted of two phases which are similar in composition, predominantly made up of Si-Mn-Fe.
- In coal 2 at 144 minutes reaction time (Figure 11), two slag phases were identified, consisting of a primary slag matrix and a crystalline phase. The slag is also associated with the alloy, which could be a result of the liquid slag penetrating into the liquid alloy with silicon carbide (SiC) distributed within the slag and alloy phases. The alloy is also characterized by a single phase consisting mainly of Si-Mn.
- The slag-anthracite boundary is clearly defined, with alloy existing mainly in between, with prills migrating into the slag. The alloy consisted of two phases; the primary alloy phase consisting of Si-Mn-Fe with Mn predominant. The anthracite did not exhibit any pores, but fine metal prills were dispersed throughout.
- At the slag-carbon interface of coal 1 (Figure 12) the slag comprised two phases, a primary phase high in CaO and $SiO_2$ and a secondary phase. The alloy consisted of two phases of Si-Mn-Fe.
- Coal 2 displays a clear contact with the slag, as seen in the coal exhibiting cracks in Figure 12. The alloy phase is characteristic of a higher Si content than Mn.
- The interface between slag and anthracite is defined by the alloy forming in between. The slag microstructure is associated with a spinel phase.
- The slag microstructure of coal 1 at 288 minutes reduction time (Figure 13) appeared different from that at 216 minutes. It consisted of a secondary slag phase of elongated crystals high in $Al_2O_3$ and CaO and no crystalline phase. Mostly metal prills were observed in the slag matrix, and hardly any large alloy particles at the reaction interface, which could indicate insufficient time for alloy particles to coalesce.
- There is no clearly defined reaction interface between coal 2 and slag. The coal integrated with the slag. The slag microstructure also appeared different, consisting of one phase with coal and alloy entrainment.
- The anthracite appeared partially consumed with large alloy particles formed, consisting predominantly of Si-Mn.
- At 360 minutes reaction time, coal 1 was porous with the slag depositing between the pores (Figure 14). The slag consisted of finely disseminated metal prills with alloy at the interface. The alloy was associated with a SiC phase, which replaces carbon as the stable carbon-containing phase.

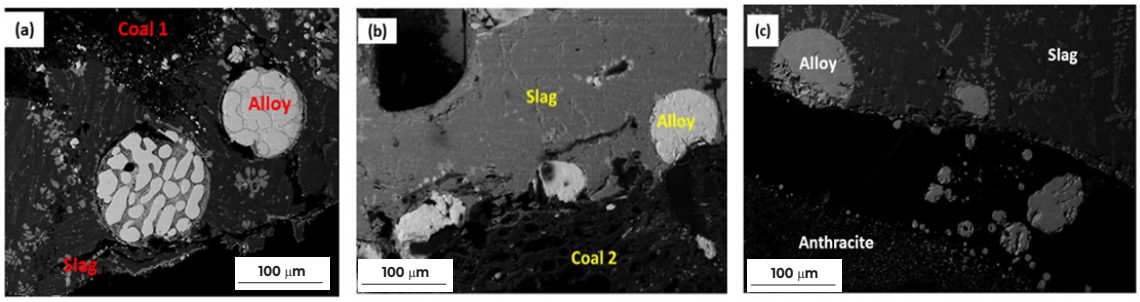


**Figure 10—SEM backscattered electron image at 72 minutes reaction time acquiredat 20.0 kV. (a) Slag, Coal 1 and alloy interface, (b) coal 2-slag interface, (c) slag-anthracite interface, Scale bar indicates 100 µm**

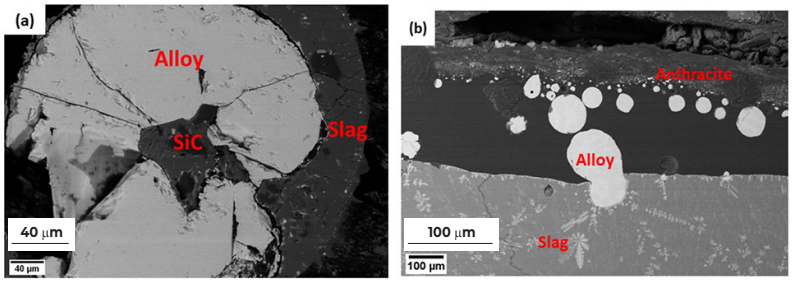


**Figure 11—SEM backscattered electron image of the interface at 144 minutes reaction time, acquired at 20.0 kV. (a) Coal 2. Scale bar indicates 40 µm. (b) Slag-anthracite interface. Scale bar indicates 100 µm**

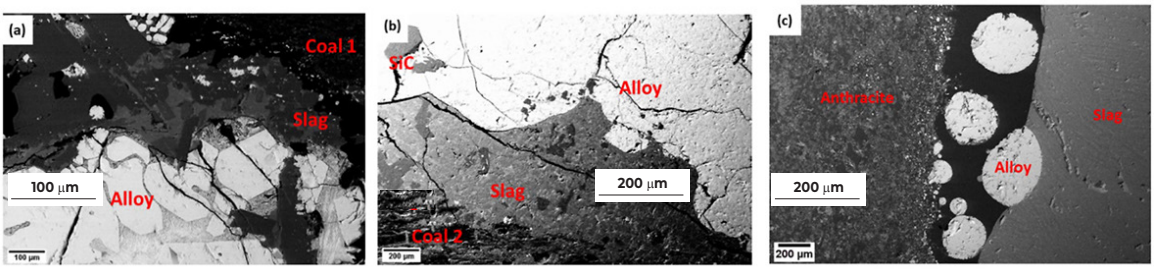


**Figure 12—SEM backscattered electron image at 216 minutes reaction time, acquired at 20.0 kV. (a) Coal 1 and slag, Scale bar indicates 100 µm. (b) Coal 2. Scale bar indicates 200 µm. (c) Anthracite-slag interface. Scale bar indicates 200 µm**

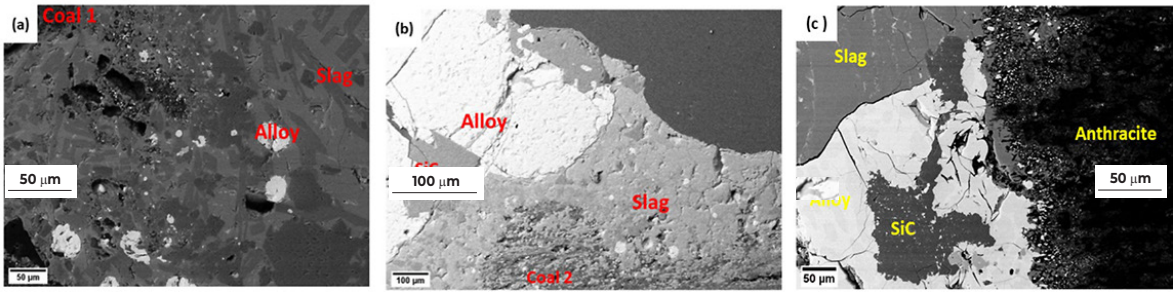


**Figure 13—SEM backscattered electron image at 288 minutes reaction time, acquired at 20.0 kV. (a) Coal 1. Scale bar indicates 50 µm. (b) Coal 2. Scale bar indicates 100 µm, (c) Anthracite. Scale bar indicates 50 µm**

- In coal 2 (Figure 14), all the coal appears to have been consumed with no clear reaction interface. The coal was either lost as volatile matter or through a reduction reaction. The slag penetrated into liquid alloy and was composed of a mixture of alloy, SiC, and slag.
- There is a clear reaction interface between slag and anthracite with the anthracite partially consumed.

Determining MnO concentrations with SEM-EDS from the slag (Table V) proved to be a challenge, especially for the two coals. The reason could be that the slag was most likely reduced from a two-phase area. Safarian and Tangstad (2010) found that for a slag reduced in a single phase, the chemical composition could be used to evaluate slag-carbon reactivity. However, this is not possible in a two-phase area. The MnO concentrations from the slag (Table V) were mostly determined from the secondary slag phase as it was difficult to determine MnO content from the primary phase.

As such, a highly reactive reductant did not equate to a faster MnO reduction rate. However, with anthracite the trend was

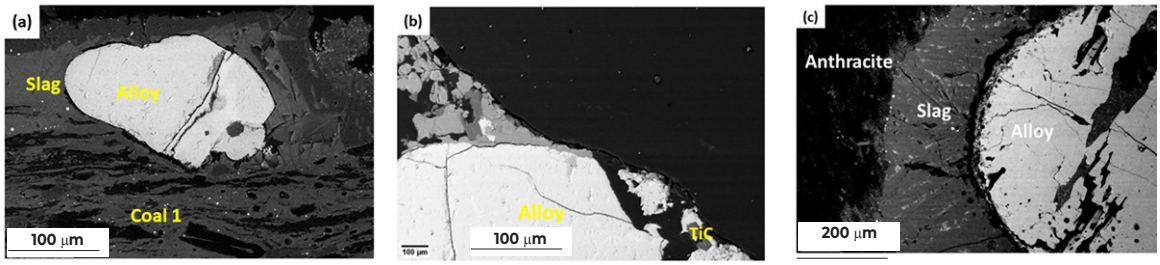


**Figure 14—SEM backscattered electron image of the slag-coal interface with alloy at 360 minutes reaction time, acquired at 20.0 kV. (a) Coal 1 and slag interface. Scale bar indicates 100 µm. (b) Slag and alloy phases. Scale bar indicates 100 µm. (c) Slag-anthracite interface. Scale bar indicates 200 µm**

more obvious, and the MnO content in the slag decreased with an increase in reduction time as seen in Table V. It was possible to determine the MnO content in slag with the anthracite samples due to the slag being present at all the reduction times with a clearly defined slag/carbon interface. This was not always the case for coal 1 and coal 2 – at longer reduction times the slag/carbon interface was not always defined and sometimes little or no slag was present.

The yield of Mn in the alloy varied, with no trend observed except for anthracite. Most of the Mn in alloy measurements were determined at the slag-carbon interface, which had a much higher Mn content than alloy surrounding slag. This is in line with the findings of Safarian and Tangstad (2010).

However, although tentative, the results did show an increase in Mn in the alloy, indicative of a reduction reaction.

Based on the above observations, a possible mechanism of MnO reduction from the slag can be proposed.

- The presence of metal prills in the slag indicates that metal is transferred from the reaction interface to the slag through gas bubbles (Tangstad and Safarian, 2010).
- The as-received slag consisted of Fe metal prills, which were occasionally found in the reduced alloy. It has been suggested that the presence of Fe metal prills increases the rate of reduction (Tranell *et al.*, 2007; Skjervheim, 1995).
- Safarian *et al.* (2009) and Tranell *et al.* (2007) observed that the presence of FeO in the slag system increases the rate of reduction. The as-received slag contained FeO, which could have played a role in the reduction of MnO. FeO is the first oxide in the system to be reduced through contact of the slag with the reductant.

*Table V*

**MnO content in slag at different reduction times (wt.%)**

| Time (min) | Anthracite | Coal 1 | Coal 2 |
|---|---|---|---|
| 0 | 21.5 | 21.5 | 21.5 |
| 72 | 18.3 | 2.0 | 17.9 |
| 144 | 18.8 | n.d. | 3.5 |
| 216 | 9.0 | 6.9 | 1.9 |
| 288 | 3.4 | 1.6 | n.d. |
| 360 | 1.8 | n.d. | n.d. |

n.d. Not determined

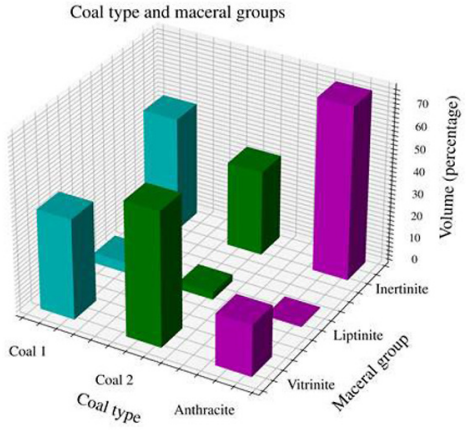


**Figure 15—Coal type and maceral groups**

## *Petrographic analysis related to reductant reactivity*

### *Effect of rank*

The reductant reactivity test results revealed that reactivity decreased with an increase in coal rank, in agreement with a study by Raaness and Gray (1995). The influence of coal rank on reactivity is associated with rank-related properties such as volatile matter and fixed carbon content (O'Keefe and Mastalerz, 2011). Generally, coal 1 and coal 2, which have high volatile matter contents and lower fixed carbon, are more reactive because of the faster rate of devolatilization. On the other hand, the higher-ranked anthracite, which devolatilizes at a higher temperature, was the least reactive.

### *Effect of maceral composition*

The organic composition showed some distinct chemical and physical differences between coals 1 and 2. The behaviour of the reductant is influenced by factors such as rank and maceral composition (Ward and Suarez-Ruiz, 2008). Coal 1 and coal 2 contained different proportions of total reactive and inertinite macerals. Coal 2, with the highest total reactive macerals (Figure 14), was the more reactive reductant. In contrast, anthracite contained the highest proportion of inertinite, and the reactivity tests confirmed that anthracite was the least reactive reductant.

The mass losses observed were due to thermal decomposition and release of volatiles, leading to changes in morphology and molecular structure of the macerals (Falcon, Wagner, and Malumbazo, 2018). Vitrinite is rich in volatile matter and hydrogen in low-rank bituminous coals. Inertinites are generally poor in volatiles. In terms of chemical reactivity, inertinite is more aromatic and richer in carbon-structured molecules (Falcon, Wagner, and Malumbazo, 2018). Anthracite, rich in inert macerals, reported lower volatile matter and thus was less reactive.

The relationship of reactive and unreactive macerals to reductant reactivity is explored through the response of the carbonaceous reductants to slag during the reactivity tests. Generally, the reductant with a higher reactive maceral content was

found to be the most reactive. Based upon the above observation, a correlation was established between petrographic parameters (coal type and rank) and reductant reactivity. The influence of devolatilization, which depends on the coal rank and proportions of volatile organic matter, was established. However, the role of the macerals in reduction could not be established as the reactivity tests could not indicate which of the individual macerals contributed to the reduction process.

## Conclusion

Coal 1 and coal 2 exhibited similar chemical properties such as volatile matter and fixed carbon content, derived from proximate analysis. Anthracite contained the least volatile matter and higher fixed carbon. The reactivity tests showed that the reductant reactivity towards slag was higher in lower ranked coals, while lower reactivity was observed in higher ranked anthracite.

Coal 1 and coal 2 were characterized by a high proportion of total reactive macerals compared to anthracite. The carbonaceous reductant reactivity towards slag showed a systematic trend, increasing with an increasing proportion of reactive macerals. The maceral analysis results showed that coal 2, with the highest proportion of reactive macerals relative to inert macerals, exhibited the highest mass loss, while anthracite, with the highest inert maceral proportions, was the least reactive. However, anthracite has low reactivity due to its high rank and high heat content. It is believed that coal rank played a larger role in the reductant reactivity than the maceral proportions. Anthracite, irrespective of maceral type, does not form porous chars (Falcon, Wagner, and Malumbazo, 2018). No information could be gathered on how the reactive and inert macerals react with the slag as a result of the reduction, but a relationship between the relative chemical reactivities of macerals and structural changes upon heating was established.

## Acknowledgements

The PreMa project is funded by the European Union's Horizon 2020 Research and Innovation Programme under Grant Agreement No. 820561 and by industry partners Transalloys, Eramet, Ferroglobe, OFZ, and Outotec. The paper is published with permission from Mintek.

## References

Alonso, M.J.G., Borrego, A.G., Alvarez, D., and Menendez, R. 2001. A reactivity study of chars obtained at different temperatures in relation to their petrographic characteristics. *Fuel*, vol .69. pp. 257–272.

Bunt, J.R., Wagner, N.J., and Waanders, F.B. 2009. Carbon particle type characterisation of the carbon behaviour impacting on a commercial-scale Sasol-Lurgi FBDB gasifier. *Fuel*, vol. 88. pp. 771–779.

Chen, P. and Ma, J. 2002. Petrographic characteristics of Chinese coals and their application in coal utilization processes. *Fuel*, vol. 81. pp. 1389-1396.

Choudhury, N., Mohanty, D., Boral, P., Kumar, S., and Hazra, S.K. 2008. Microscopic evaluation of coal and coke for metallurgical usage. *Current Science*, vol. 94. pp. 74–81.

Coetsee, T. 2018. Ore smelting in high carbon ferromanganese production: "It works in practice, but does it work in theory?" *Proceedings of INFACON XV: International Ferro-Alloys Congress*, Cape Town, 25-28 February 2018. Southern African Institute of Mining and Metallurgy, Johannesburg. pp.1–13.

Diessel, C.F.K. 1992. Coal-bearing Depositional Systems. Springer, Berlin.

Falcon, R. and Ham, A.J. 1988. The characteristics of Southern African coals. *Journal of the South African Institute of Mining and Metallurgy*, vol. 88, no. 5. pp. 145–161.

Falcon, R., Wagner, N., and Malumbazo, N. 2018. Southern African Coals and Carbons: Definitions and Applications of Organic Petrology. 1st edn. Struik Nature, Cape Town.

International Organization for Standardization. 1994. Method for the petrographic analysis of bituminous coal and anthracite-: Preparation of coal samples. ISO Standard 7404 Part 2. ISO Standards.

International Organization for Standardization. 1994. Method for the petrographic analysis of bituminous coal and anthracite: Method for determining maceral group composition. ISO Standards 7404 Part 3. ISO Standards.

Kim, P.P. 2018. Reduction rates of SiMn slags from various raw materials. PhD Thesis, Norwegian University of Science and Technology.

Kolbeinsen, L., Safarian, J., Grong, O., and Olsen, S.E. 2006. A process model for the carbothermic reduction of MnO from high carbon ferromanganese slag - The model. *ISIJ International*, vol. 46, no. 8. pp. 1120–1129.

Lindstad, T., Tangstad, M., and Olsen, S.E. 2007. Production of Manganese Ferroalloys. Tapir Academic Press, Trondheim.

Malumbazo, N., Wagner, N.J., and Bunt, J.R. 2012. The petrographic determination of reactivity differences of two South African inertinite-rich lump coals. *Journal of Analytical and Applied Pyrolysis*, vol. 93. pp. 139–146.

O' Keefe, J.M.K., Betchel, A., Christanis, K., Dai, S., DiMichele, W.A., Eble, C.F., Esterle, J.S., Mastalerz, M., Raymond, A.L., Valentim, B.V., Wagner, N.J., Ward, C.R., and Hower, J. 2013. On the fundamental differences between coal rank and coal type. *International Journal of Coal Geology*, vol. 118. pp. 58–87.

Olsen, S.E. and Tangstad, M. 2004. Silicomanganese production-process understanding. *INFACON X: Transformation Through Technology. Proceedings of the Tenth International Ferroalloys Congress*, Cape Town. pp. 231–238. https://www.pyrometallurgy.co.za/InfaconX/012.pdf

Olso, V., Tangstad, M., and Olsen, S.E.1998. Reduction kinetics of MnO saturated slags. *Proceedings of INFACON 8*. pp.279–283. https://www.pyro.co.za/InfaconVIII/279-Olso.pdf

Ostrovski, O. and Swinbourne, D. 2013. Slags in production of manganese alloys. *Steel Research International*, vol. 84, no. 7. pp. 680–686.

Pinheiro, H. 2006. Springlake anthracite - Characterisation and potential industrial utilisation. PhD thesis, Universidade do Porto, Portugal.

Pistorius, P.C. 2002. Reductant selection in ferroalloy production: The case for the importance of dissolution in the metal. *Journal of the South African Institute of Mining and Metallurgy*, vol. 102, no. 1. pp. 33–36.

Rankin, W.J. and van Deventer, J.SJ. 1980. The kinetics of reduction of manganese oxide by graphite. *Journal of the South African Institute of Mining and Metallurgy*, vol. 80. pp. 239–247.

Rankin, W.J. and Wynnyckyj, J.R. 1997. Kinetics of reduction of MnO in powder mixtures with carbon. *Metallurgical and Materials Transactions B*, vol. 28B. pp. 307–319.

Ringdalen, E., Tangstad, M., and Gaal, S. 2009. Initial melting and reduction of ore and fluxes at the top of the coke bed during SiMn-production. P*roceedings of the VIII International Conference on Molten Slags, Fluxes & Salts*, Santiago, Chile, 18-21 January 2009. Sánchez, M., Parra, R., Riveros, G., and Díaz, C. (eds). Universidad de Concepción, Department of Metallurgical Engineering, pp. 1164–1172. *Molten 2009.*

Ringdalen, E., Tangstad, M., and Brynjulfsen, T. 2015. Melting behaviour of Mn sources - Effect on furnace performance. *Proceedings of the Fourteenth International Ferroalloys Congress: Energy Efficiency and Environmental Friendliness are the Future of the Global Ferroalloy Industry*, Kiev, pp. 436–445. https://www.pyrometallurgy.co.za/InfaconXIV/436-Ringdalen.pdf

Raanes, O. and Gray, R.J. 1995. Coal production of silicon rich ferroalloys. *Proceedings of INFACON 7*, Trondheim, Norway, pp. 201-220. https://www.pyrometallurgy.co.za/InfaconVII/201-Raaness.pdf

Safarian, J. and Kolbeinsen, L. 2008. Kinetic of carbothermic reduction of MnO from high-carbon ferromanganese slag by graphite materials. *ISIJ International*, vol. 48, no. 4. pp. 395–404.

Safarian, J., Kolbeinsen, L., Tangstad, M., and Tranell, G. 2009. Kinetics and mechanism of the simultaneous carbothermic reduction of FeO and MnO from high-carbon ferromanganese slag. *Metallurgical and Materials Transactions B*, vol. 40B. pp. 929–939.

Sahajwalla, V., Dubikova, M., and Khanna, R. 2004. Reductant characterisation and selection: Implications for ferroalloys processing. *Proceedings of INFACON X: Transformation through Technology*, Cape Town, South Africa. pp. 351–362. https ://www.pyrometallurgy.co.za/InfaconX/049.pdf

Skjervheim, T. and Olsen, S.E. 1995. The rate and mechanism for reduction of manganese oxide from silicate slags. *Proceedings of INFACON 7*, Trondheim, Norway. pp. 631–639. https://www.pyro.co.za/InfaconVII/631-Skjervheim.pdf

Speight, J.G. 2015. Handbook of Coal Analysis. Wiley.

Suharno, B., Nurjaman, F., Rifki, A., Elvin, R.K., Putra, A.A., and Ferdian, D. 2018. Coke and coals as reductants in manganese ore smelting: An experiment. *Mineralogia*, vol. 49, no. 1-4. pp. 35–45.

Suarez- Ruiz, I. and Ward, C.R. 2008. Introduction to applied coal petrology. *Applied Coal Petrology*. The Role of Petrology in Coal Utilization. Elsevier, Amsterdam. pp. 2–18.

Tangstad, M., Steenkamp, J.D., Ringdalen, E., and Beukes, J.P. 2019. Coal based reducing agents in ferroalloys and silicon production. *New Trends in Coal Conversion: Combustion, Gasification, Emissions and Coking*. Woodhead Publishing. pp. 405–435.

Teasdale, S.L. and Hayes, P.C. 2005. Kinetics of reduction of FeO from slag by graphite and coal chars. *ISIJ International*, vol. 45, no. 5. pp. 642–650.

Tranell, G., Gaal, S., Lu, D., Tangstad, M., and Safarian, J. 2007. Reduction kinetics of manganese oxide from HC FeMn slags. *Proceedings of INFACON XI*. pp. 232–240. https://www.pyrometallurgy.co.za/InfaconXI/231-Tranell.pdf

United Nations Economic Commission for Europe. 1998. International classification of in-seam coals. Geneva. ◆